Waste Biomass Valor (2014) 5:305–313
DOI 10.1007/s12649-013-9257-4

ORIGINAL PAPER

E. grandis as a Biocarbons Precursor for Supercapacitor Electrode Application

Andrés Cuña · Nestor Tancredi · Juan Bussi · Ana Cristina Deiana · Maria Fabiana Sardella · Violeta Barranco · José M. Rojo

Received: 10 January 2013 / Accepted: 28 June 2013 / Published online: 9 July 2013

Abstract Wood residues are ordinary wastes in the forestry industry and their valorization is an important issue. *Eucalyptus grandis* wood dust was chosen as a model wood residue and biocarbons (BCs) and activated BCs were prepared from it and studied as active materials for supercapacitor electrodes. Several ordinary activation methods were used and microporous activated BCs with specific surface areas up to 900 m^2 g^{-1}, and different content of oxygenated surface groups were obtained. The preparation or activation temperature is the parameter that mainly affects the electrical conductivity. For temperatures above 700 °C, the samples reach an electrical conductivity as high as 1 S cm^{-1}. The specific capacitance of the activated BCs reaches values up to 203 F g^{-1} in acidic electrolyte. The highest specific capacitance is obtained when chemical activation with $ZnCl_2$ at 900 °C followed by chemical oxidation with nitric acid is used. BCs activated with $ZnCl_2$ at 900 °C and CO_2 at 800 °C displayed good rate capability and the maximum power density. Activation with $ZnCl_2$ at 900 °C also leads to BCs with the maximum energy density. These results show that *E. grandis* wood dust is a promising low cost and environmental friendly precursor for biocarbon electrodes.

Keywords Wood residues · Energy storage · Supercapacitors · Activated carbons · Biocarbons · *Eucalyptus grandis* wood

A. Cuña (✉) · N. Tancredi · J. Bussi
Cátedra de Fisicoquímica, Laboratorio de Fisicoquímica de Superficies, DETEMA, Facultad de Química, Universidad de la República, General Flores 2124, CC 1157, 11800 Montevideo, Uruguay
e-mail: acuna@fq.edu.uy

A. C. Deiana · M. F. Sardella
Facultad de Ingeniería, Instituto de Ingeniería Química, Universidad Nacional de San Juan, Av. Libertador 1109, 5400 San Juan, Argentina

V. Barranco · J. M. Rojo
Instituto de Ciencia de Materiales de Madrid (ICMM), Consejo Superior de Investigaciones Científicas (CSIC), Sor Juana Inés de la Cruz, 3, Cantoblanco, 28049 Madrid, Spain

Introduction

Wood residues are ordinary wastes in the forestry industry. In Uruguay, recent estimations of the amount of forest residues for the period 2012–2020 indicate that sawmill residues are more than 1,000,000 m^3 per year (450,000 tons), while forest residues range between 1.2 and 1.8 million m^3 per year (1–1.5 million ton). The valorization of these residues is then an important issue both from the technical and the economical viewpoint. One way for this valorization is the preparation of activated carbon from them and the utilization of the prepared activated carbon as active electrode materials for supercapacitors.

Supercapacitors are promising electrochemical energy storage devices with important advantages over batteries, including higher power density and larger number of charge/discharge cycles. They have found applications in electric transportation technologies, emergency backup power and grid system stability, in fuel cells and eolic energy generation [1–3].

Specific energy storage in supercapacitors is proportional to the specific electrical capacitance of the active material electrodes, which is influenced by their textural properties and the amount of the electrochemically active surface functional groups. Dealing with textural properties, large specific surface areas and suitable pore size distributions are

required to maximize the double layer capacitance. Although mesopores in the range of 2–5 nm were considered to be more appropriate than micropores to act as reservoirs for the electrolyte ions in mixed microporous/mesoporous materials [4], the finding that the electrolyte ions can be accommodated into the micropores as desolvated or partially desolvated ions arouse new interest on microporous materials [2]. Pseudocapacitive contribution, which comes from reversible redox reactions at the electrode surface, is strongly dependent on the nature of the active electrode materials. Metal oxides, conducting polymers, and carbons have been extensively studied in the last decades for those purposes [1, 3, 5].

Other physical–chemical properties must be taken into account to improve the performance of supercapacitors. In particular, high electrical conductivity is an important property to provide high power density, and no chemical reactivity to reach long cycle life [6, 7]. Additionally, low cost and environmentally friendly materials should contribute to satisfy requirements of the massive use of supercapacitors in the future.

Carbons and activated carbons are the most widely used materials for supercapacitor electrodes [2, 3, 7, 8] because they can satisfy all the requirements for this application: high specific surface area, open porosity, high conductivity, electrochemical stability and moderate low cost. In addition, carbon materials are almost invariably associated with an appreciable concentration of surface functional groups, containing oxygen, hydrogen, and to a lesser degree, nitrogen, sulfur and halogens which can participate in pseudocapacitive redox reactions [8–11]. These functional groups may also be incorporated onto the carbon surface by different types of physical or chemical treatments. Recent studies have identified some correlations between pseudocapacitance and the amount of surface functional groups generating CO and CO_2 in temperature-programmed desorption (TPD) [9, 12, 13].

Activated carbons are currently prepared from a precursor, such as a polymer, a mineral carbon or some kind of biomass wastes [14]. Regarding the latter, biomass wastes are a renewable source, available in large amounts, and still at low cost [15–17]. The use of biomass derived carbons (biocarbons) as active electrode materials for supercapacitors has been reported in the last years [5, 15, 18–20]. The biomass nature and the activation method determine the electrochemical performance, with textural properties, electrical conductivity and electrochemical active surface functional groups all affecting the overall capacitance.

Eucalyptus wood is a tree cultivated over the world that shows the advantage of its rapid growing. Its wood is currently used for manufacturing furniture and for obtaining cellulose paste and allows the preparation of activated carbons with high microporosity [17, 21–25]. The use of this wood as biocarbon precursor for supercapacitor electrode application has not been reported yet.

In this work, *Eucalyptus grandis* wood dust was chosen as carbon precursor, as a model wood residue, and biocarbons (BCs) and activated BCs were obtained by several procedures. Their textural, chemical and electrical properties were determined. They were also tested as active electrode materials for supercapacitors.

Materials and Methods

Sample Preparation

BCs and activated BCs were obtained from *E. grandis* wood dust, which was chosen as a biomass precursor. Wood carbonization, chemical or physical activation, or oxidation were performed under experimental conditions usually employed in previous studies [14]. A summary of the preparation procedures including oxidizing or activating agents, temperatures and times is shown in Table 1. The preparation or activation parameters, i.e. procedure, reagents, temperature and time are shown in the corresponding columns. Concentration of the chemical agent in the aqueous solution expressed as mass percentage (%). E.g. stands for *E. grandis* wood dust as starting material. Other samples (C300, C650, M9, M12 and M13) were also chosen as starting materials. These samples were also obtained from the *E. grandis* precursor.

In some particular cases, the already obtained activated BCs were additionally oxidized in nitric acid or heat treated under nitrogen flow. All the thermal treatments were carried out in a horizontal Carbolite (CTF 12/75) furnace under a controlled gas flow. The gases used were: nitrogen of 99.998 % purity, carbon dioxide of 99.98 % purity, and air. The flow of the three gases was of 200 cm^3 min^{-1}. For carbonizations, the samples obtained were labelled as *C* followed by the temperature applied, in Celsius degree, e.g. C500. All chemicals were of analytical grade. For chemical activations, aqueous solutions of the activating agent were prepared. The activating agent solution/wood weight ratio was 7/1 for LiOH, 5/1 for H_3PO_4, 6/1 for KOH, and 1/1 for $ZnCl_2$. After the chemical activations, the samples were washed with distilled water up to neutral pH of the washing water, and then dried in still air at 105 °C for 24 h. In some particular cases, the chemically activated BCs were additionally heated under nitrogen flow at 1,030 °C for 11 h. They are heat treated samples, labelled as the name of the activated carbons followed by +TT.

X-ray Diffraction

The X-ray diffractograms were obtained on a Bruker D8 Advance XRD diffractometer, using Cu-K_α radiation.

Table 1 Preparation of biocarbons and activated biocarbons

Sample	Activation method or sample treatment	Activating agent	Temperature (°C)	Time (h)	Starting material
M1	Physical	CO_2	800	1	E.g.
M2	Physical	CO_2	800	2	E.g.
M3	Physical	CO_2	800	1	C300
M4	Physical	CO_2	800	1	C650
M5	Physical	Air	400	1	E.g.
M6	Physical	Air	400	2	E.g.
M7	Physical	Air	400	1	C300
M8	Physical	Air	400	1	C650
M9	Chemical	H_3PO_4 28 %	350	1	E.g.
M10	Chemical	H_3PO_4 28 %	650	1	E.g.
M11	Chemical	KOH 50 %	650	1	E.g.
M12	Chemical	LiOH 9 %	650	1	E.g.
M13	Chemical	$ZnCl_2$ 80 %	900	1	E.g.
C300	Carbonization	–	300	2	E.g.
C350	Carbonization	–	350	2	E.g.
C500	Carbonization	–	500	2	E.g.
C550	Carbonization	–	550	2	E.g.
C650	Carbonization	–	650	2	E.g.
C900	Carbonization	–	900	2	E.g.
M9 + TT	Thermal treatment	–	1,030	11	M9
M12 + TT	Thermal treatment	–	1,030	11	M12
M13 + TT	Thermal treatment	–	1,030	11	M13
M14	Chemical oxidation in HNO_3 4 M	–	83	1.5	M13

Textural Characterization

The porous texture of 18 samples was studied by N_2 adsorption/desorption isotherms at 77 K, performed by a Micromeritics ASAP 2010. The analysis by application of the Dubinin–Radushkevich equation led to the volume of the micropores, W_0, the average micropore width, L_0, and the micropore surface area, S_{mic}. The external surface area (i.e. non-microporous), S_{ext}, was deduced from comparison with a non-porous carbon used as reference (*Vulcan* 3G). Then, the total surface area was calculated as $S_{mic} + S_{ext}$. In order to get a reliable determination of the specific surface areas, the nitrogen adsorption isotherms were also analyzed by other methods such as the comparison plot, S_{comp}. The average surface area (S_{av}) was calculated as $S_{av} = [(S_{mic} + S_{ext}) + S_{comp}]/2$ [26–28].

TPD Experiments

For 18 samples, Temperature-Programmed Desorption (TPD) experiments were performed in DTA-TGA equipment (TA instruments, SDT Q600) coupled to a mass spectrometer (Thermostar, Pfeiffer, TM GSD 301T). The amounts of CO and CO_2 evolved from the samples were determined during the heating up to 900 °C (heating rate of 5 °C min^{-1}) under a dry argon flow (100 cm^3 min^{-1}). The contents of CO and CO_2 are referred to the weight of sample. The weight of every sample was 10-20 mg. $CaC_2O_4{\cdot}H_2O$ was used as a calibration standard for the intensities of the CO and CO_2 signals.

Electrical Conductivity Measurements

Electrical conductivity of the BCs and activated BCs was measured on pellets that were processed as composites. Polyvinylidene fluoride (PVDF), a widely used binder inert against the aqueous electrolyte H_2SO_4 and with a very low electrical conductivity, was added for improving the pellet handling. The PVDF content (10–15 wt% of the pellet weight) was chosen as the minimum amount required for obtaining handled pellets. This quantity is lower than the percolation threshold, therefore the composite electrical conductivity is dominated by that of the carbon. In some particular cases, a small amount of carbon black, CB (5–10 wt% of the pellet weight) was added to check the effect of this component on the electrical conductivity of the pellet. The pellets of 6 mm in diameter, 1.0–1.5 mm in thickness, and 40-50 mg in weight were obtained after cold

pressing at 10 MPa. Two-probe AC measurements were carried out in a 1260 Solartron gain-phase analyzer (frequency range 1 Hz–1 MHz) at room temperature. Silver paint was applied at the two circular surfaces of the pellets. Electrical conductivity was calculated according to $\sigma = h{\cdot}R^{-1}{\cdot}A^{-1}$; where R is the resistance measured, h is the pellet thickness and A is the circular surface area.

Electrochemical Measurements

Two-electrode Swagelok™-type cells having two tantalum rods as current collectors were used. A glassy microfibre paper (Whatman 934 AH) was used as separator. The electrodes (50–120 mg) were prepared by mixing the carbon sample (70–75 wt%), PVDF (15–20 wt%) and CB (10–15 wt%). The three components were mixed and ground in an agate mortar. Then, cylindrical pellets of 6 mm in diameter and 1–2 mm in thickness were obtained after cold pressing at 10 MPa. Eighteen samples were studied in 2 M aqueous H_2SO_4 electrolyte. The specific capacitance was measured at room temperature by a 1286 Solartron potentiostat/galvanostat. Galvanostatic charges and discharges were performed at a current density in the range 1–200 mA cm^{-2}. The specific capacitance was determined according to the equation: $C = 2{\cdot}I{\cdot}t_d/E_2{\cdot}m_e$, where I is the current applied, t_d is the discharge time, E_2 is the voltage range during the discharge, and m_e is the mass of the carbon sample in one electrode. Cyclic voltammetries were performed at voltage scan rates of 1, 2 and 5 mV s^{-1}. Both galvanostatic and voltammetric measurements were carried out at room temperature in the voltage range of 0–1 V.

Results and Discussion

Textural and Chemical Surface Characterization

Table 2 summarizes the results obtained of the total surface area (S_{av}), microporous surface area (S_{mic}), average pore width (L_0) and contents of surface functional groups generating CO and CO_2 in TPD, named here-after as [CO] and [CO_2]. A wide variation of S_{av}, from 42 to 908 m^2 g^{-1}, was found. This is a consequence of the variety of preparation methods used, that included different temperatures, activating agents and activation times [14]. S_{av} is close to S_{mic} in agreement with the fact that all the carbons are microporous. Indeed, L_0 ranges from 0.6 to 2.0 nm. Samples in Table 2 are ordered according to the S_{av}, and in order to facilitate the discussion they were grouped into two groups: A for samples with $S_{av} < 400$ m^2 g^{-1} and B for samples with $S_{av} > 400$ m^2 g^{-1}. Activated BCs in group A were obtained by activation with LiOH (M12 and M12 + TT), air (M5, M6 and M7) and H_3PO_4 (M10). The low S_{av} which was found for M12 is probably due to a strong attack of the LiOH under the experimental conditions here used [29]. The heat treatment under N_2 flow at 1,030 °C led to a decrease of S_{av}. Thus, the M12 + TT sample shows $S_{av} = 42$ m^2 g^{-1} while the starting sample M12 shows $S_{av} = 193$ m^2 g^{-1}. The decrease in S_{av} can be associated with removal of a part of the micropores and contraction of the carbon structure. Group A also contains the non-activated BCs (C500, C650 and C900), and their low S_{av} values (from 283 to 351 m^2 g^{-1}), are in agreement with the results reported for others BCs [30]. Among the activated BCs in group B, those obtained by activation with $ZnCl_2$ (M13 and M14) display the largest S_{av} (843 and 838 m^2 g^{-1} respectively). The oxidation in HNO_3 did not change significantly the S_{av} value. It can be seen that the heat treatment of samples activated with H_3PO_4 (M9) and activated with $ZnCl_2$ (M13) led to an increase of surface area, that can be explained on the basis of a portion of the activating agent still remaining in the activated BCs M9 and M13 after washing with distilled water. So, the subsequent heating under N_2 flow continued the activation.

Regarding the contents of oxygenated functional groups, the samples that were prepared at temperatures below 700 °C, including chemically activated and air-oxidized samples, showed higher content of oxygenated functional groups than the samples that were prepared above 700 °C, i.e. physically and chemically activated samples as well as heat treated samples. Air oxidized samples (M5, M6 and M7) showed oxygenated groups contents close to those of BCs as their activation temperatures were close to the carbonization ones. As an example, the C500 sample shows [CO] = 3.78 mmol g^{-1} and [CO_2] = 0.74 mmol g^{-1}, which are close to those found for M5, M6 and M7 (see Table 2.). The high content of oxygenated functional groups found for the air activated BCs can be due to carbon–oxygen reactions involved in the activation process [31].

Correlation of Electrical Conductivity and Preparation Temperature

Figure 1 shows the dependence of the electrical conductivity as a function of the preparation temperature. A variation by more than 8 orders of magnitude is observed. It can be noted that the sharp increase of conductivity happens in the range 500–700 °C. Conductivity changes from 10^{-8} S cm^{-1} for temperatures below 500 °C to 1 S cm^{-1} for temperatures above 700 °C. In the case of the M8, although it was activated at 400 °C its precursor (C650) had been obtained at 650 °C; consequently its conductivity is higher than that of other samples prepared at 400 °C. The high electrical conductivity observed for the samples obtained at high temperature can be explained on the basis of a higher structural order of the aromatic structure with

Table 2 Textural, TPD results and specific capacitance of the BCs and activated BCs

Group	Sample	Textural analysis							TPD results		Specific capacitance C_1 (F g^{-1})
		W_o (cm^3 g^{-1})	L_o (nm)	S_{mic} (m^2 g^{-1})	S_{ext} (m^2 g^{-1})	$S_{mic} + S_{ext}$ (m^2 g^{-1})	S_{comp} (m^2 g^{-1})	S_{av} (m^2 g^{-1})	[CO] (mmol g^{-1})	[CO_2] (mmol g^{-1})	
A	M12 + TT	–	≈>2	–	–	–	42	42	0.11	0.24	13
	M6	0.03	1.19	50	≈0	50	50	50	2.72	1.25	61
	M10	0.13	1.93	135	7	142	167	155	5.59	0.65	119
	M12	0.11	1.50	147	34	181	205	193	5.12	0.86	75
	M7	0.10	0.84	238	1	239	243	241	3.17	0.66	70
	C500	0.18	1.28	281	2	283	282	283	3.78	0.74	40
	M5	0.12	0.83	289	2	291	280	286	3.00	0.84	69
	C900	0.12	0.86	279	1	280	315	297	1.05	0.46	32
	C650	0.13	0.70	371	3	374	328	351	1.96	0.84	56
B	M9	0.28	1.39	403	12	415	466	441	2.25	1.31	125
	M11	0.17	0.76	447	13	460	453	457	1.65	2.18	128
	M9 + TT	0.30	1.02	588	8	596	604	600	0.33	0.21	100
	M2	0.24	0.68	706	11	717	705	711	0.28	0.64	125
	M1	0.26	0.74	703	14	717	716	717	0.52	0.96	140
	M3	0.23	0.59	780	3	783	764	774	0.80	0.54	135
	M14	0.49	1.26	778	2	780	897	838	2.77	1.95	203
	M13	0.48	1.17	821	2	823	863	843	0.49	0.24	177
	M13 + TT	0.52	1.14	912	7	919	897	908	0.05	0.08	190

conjugation and π bonds; that facilitate the motion of electrons. Figure 2 displays X-ray diffractograms of BCs, activated BCs and heat treated samples, which were obtained at increasing temperature. Two broad peaks appear at approximately $2\theta = 25°$ and 44°. For the BCs, the peak at $2\theta = 44°$ became more intense as the preparation temperature increased. It indicates that carbonization at high temperature tends to produce a more organized aromatic carbon with marked sp^2 bonding character than the amorphous-like carbon with higher sp^3 bonding character prepared at a lower temperature [30, 32, 33]. In a lesser extent, differences in the electrical conductivity can also be observed for activated BCs obtained at the same preparation temperature with different activating agents (Fig. 1). Differences from one to three orders of magnitude can be observed for the M8, M10, M11 and M12 sample, which were obtained at 650 °C. Similar differences are found for the M13, M14 and C900 samples, which were obtained at 900 °C. On one hand, these differences in conductivity can be associated with the presence of oxygenated groups at the carbon surface and their negative contribution to the electrical conductivity [34]. On the other hand, changes in microporous volume as well as in pore diameter can affect the electrical conductivity measured.

Figure 1 also shows that the addition of carbon black (CB), which is commonly used to improve electrical conductivity of supercapacitor electrodes, can affect differently the electrical conductivity of the samples. For instance, for the M7 biocarbon showing a low conductivity (10^{-8} S cm^{-1}), the addition of carbon black made it

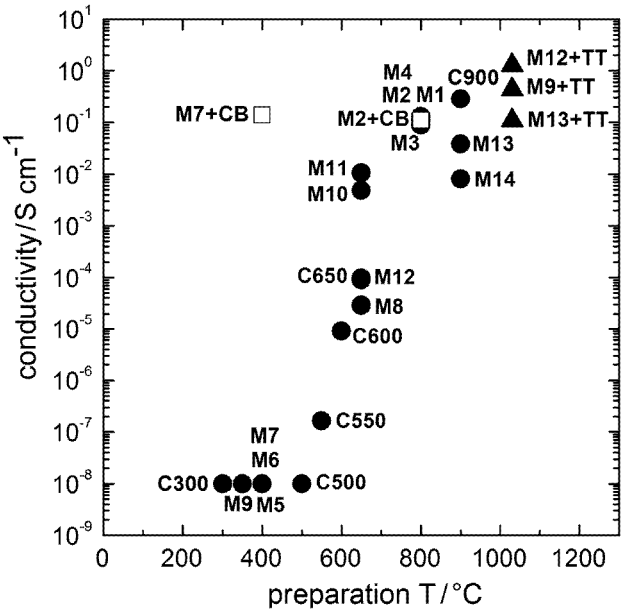

Fig. 1 Electrical conductivity versus preparation temperature for the BCs and activated BCs (*filled circles*), heat treated carbons (*filled triangles*), and carbons with a small amount of carbon black added (*open squares*)

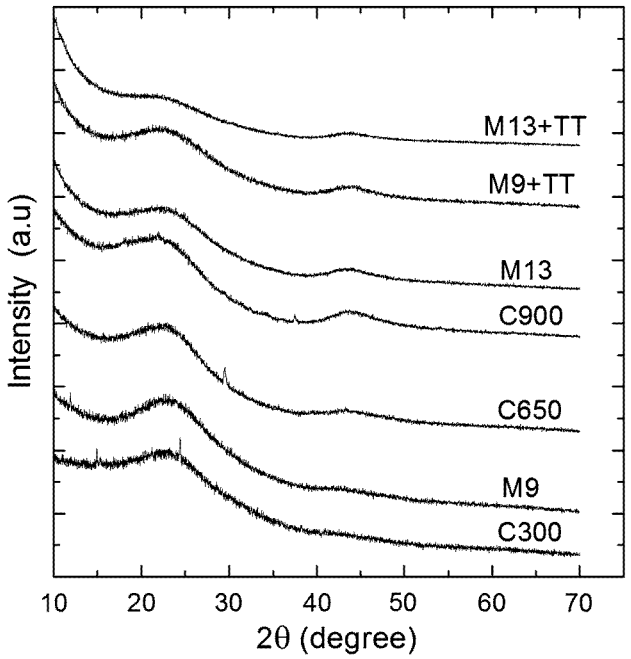

Fig. 2 X-ray diffractograms of several BCs and activated BCs

possible to increase the electrical conductivity by 7 orders of magnitude, up to 10^{-1} S cm^{-1} (see M7 + CB in Fig. 1). However, the addition of CB to the M2 sample did not change the electrical conductivity, which is ca. 10^{-1} S cm^{-1} for both M2 and M2 + CB. This is due to the fact that the electrical conductivity of M2 is close to that of CB.

From the point of view of using the carbons prepared in this work as supercapacitor electrodes, the carbons obtained at temperatures below 700 °C show a low electrical conductivity, and consequently they are not suitable as electrode materials. However, these carbons can display other interesting characteristics such as a large specific surface area and a significant content of oxygenated groups, both characteristics favouring a high specific capacitance. Then, these carbons could be used as electrodes if a small amount of CB is added. The samples prepared at temperatures above 700 °C, show high electrical conductivity, and hence they can be used as supercapacitor electrodes without any CB addition.

Electrochemical behaviour of the BCs and activated BCs as supercapacitor electrodes

It is well known that the specific capacitance has two components: the double layer capacitance, directly related to the specific surface area, and the pseudocapacitance, related to the content of surface functional groups capable of participate in reversible redox reactions [1–3]. According to the former criterion, the BCs and activated BCs are grouped into two groups, as it was stated before. Then, the influence of the content of oxygenated functional groups on the specific capacitance is discussed for some particular cases.

For group A, the specific capacitances are lower than 100 F g^{-1}. This result agrees with the low S_{av} values although in some samples the content of oxygenated functional groups evolved as CO is high. There is one exception; M10 with a specific capacitance of 119 F g^{-1}, which was obtained by activation with H_3PO_4 at 650 °C. A high pseudocapacitance contribution is expected for this sample according to its relatively high content of oxygenated functional groups ([CO] = 5.59 mmol g^{-1} and [CO_2] = 0.65 mmol g^{-1}). Besides the pseudocapacitance due to the oxygenated surface groups, a pseudocapacitive contribution could be caused by the presence of phosphate and polyphosphate functional groups [35].

For group B, specific capacitances are higher than 100 F g^{-1}, which agree with the higher S_{av} values. These activated BCs were obtained by activation with $ZnCl_2$ (M13 and derivatives M13 + TT and M14), by activation with CO_2 (M1, M2 and M3) and also by activation with H_3PO_4 (M9, M9 + TT) and with KOH (M11). The $ZnCl_2$ activated samples exhibit specific capacitances (177–203 F g^{-1}) higher than the other samples. The good results observed for activation with $ZnCl_2$ are in agreement with those reported by Rufford et al. [15, 19], also for biomass activation. The highest specific capacitance (203 F g^{-1}) was found for the M14 sample, which was obtained from the M13 sample after further nitric acid oxidation. Taking into account that the M13 and M14 sample have close specific surface areas (843 and 838 m^2 g^{-1}, respectively), the higher specific capacitance of the M14 sample can be explained by the higher pseudocapacitive contribution associated with the higher content of oxygenated functional groups. Indeed, the TPD results (Table 2) show higher content of oxygenated functional groups desorbed as CO and CO_2 for M14 ([CO] = 2.77 mmol g^{-1} and [CO_2] = 1.95 mmol g^{-1}) than for M13 ([CO] = 0.49 mmol g^{-1} and [CO_2] = 0.24 mmol g^{-1}). Moreover, in Fig. 3, the voltammogram obtained for M14 shows a broad peak, between 0.2 and 0.5 V, which is typical of redox reactions of oxygenated surface functional groups. The increase of the pseudocapacitance after nitric acid oxidation agrees with the results reported for other carbonaceous materials [9, 36]. CO_2 activated BCs (M1, M2 and M3) show specific capacitances ranging from 125 to 140 F g^{-1}, slightly lower than the aforementioned activated BCs. The decrease in specific capacitance is in agreement with their lower specific surface areas (9–15 % lower) and their lower content in oxygenated functional groups when compared to M14. The M9 and M2 activated BCs show the same specific capacitance, 125 F g^{-1}. The M2 sample shows a larger specific surface

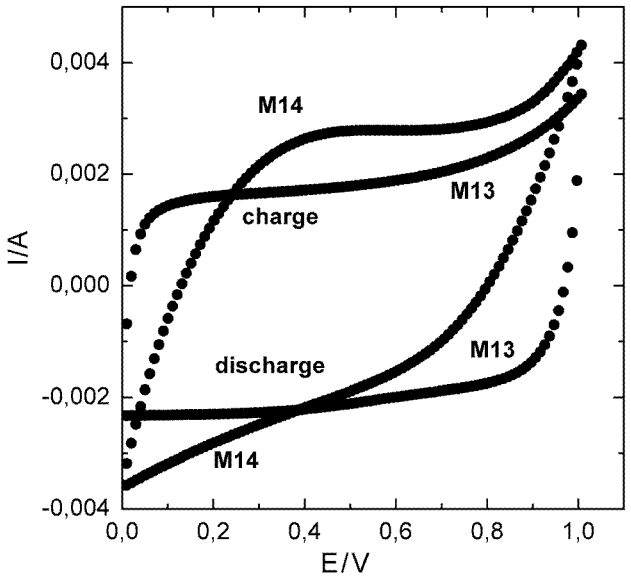

Fig. 3 Cyclic voltammetries obtained in aqueous 2 M H_2SO_4 electrolyte for the activated BCs M13 and M14, at 1 mV s^{-1} scan rate

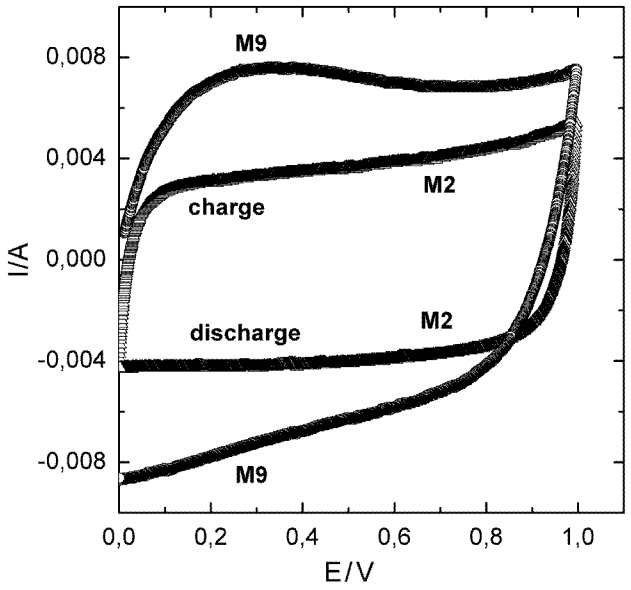

Fig. 4 Cyclic voltammetries obtained in aqueous 2 M H_2SO_4 electrolyte for the activated BCs M2 and M9, at 2 mV s^{-1} scan rate

area, and consequently higher double layer capacitance. The M9 sample shows higher content of oxygenated functional groups, and then higher pseudocapacitance. This fact is confirmed by the cyclic voltammogram shown in Fig. 4, where broad peaks between 0.2 and 0.5 V are clearly observed for the M9 sample. Both contributions, double layer capacitance and pseudocapacitance, are balanced in such a way that they lead to the same specific capacitance for both samples.

The dependence of the specific capacitance as a function of the current density for some activated BCs is shown in

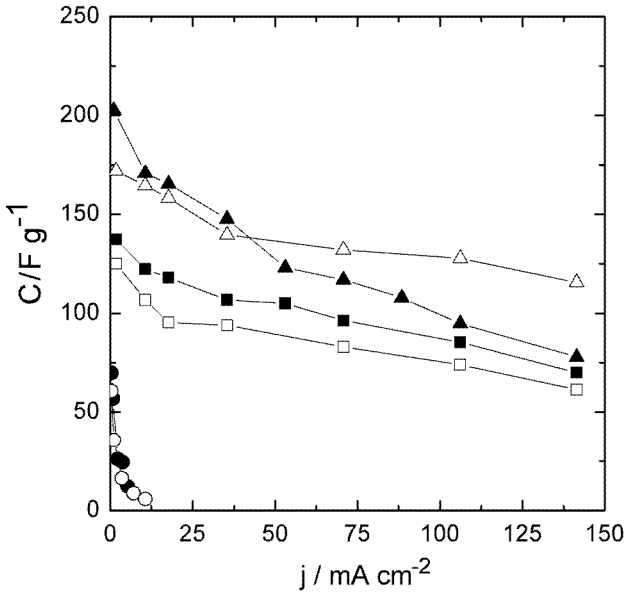

Fig. 5 Specific capacitance vs. current density for some activated biocarbons in aqueous 2 M H_2SO_4 electrolyte. Symbols stand for as follows: *filled triangles* for M14, *open triangles* for M13, *filled squares* for M1, *open squares* for M2, *filled circles* for M5 and *open circles* for M6

Fig. 5. The M5 (filled circles) and M6 (open circles) samples have in common a low specific surface area and high content of oxygenated functional groups. At low current density (1 mA cm^{-2}), the specific capacitance is low, which is consistent with their low S_{av}; the pseudocapacitive contribution must be high, according to their high content in oxygenated functional groups desorbed as CO and CO_2. At higher current densities (>1 mA cm^{-2}), the specific capacitance decreases strongly as the current density increases. This significant decrease is associated with the high content of oxygenated functional groups of those samples. The samples M1 (closed squares) and M2 (open squares) have larger S_{av} (717 and 711 m^2 g^{-1}) but lower contents of oxygenated functional groups. At low current density, their specific capacitance is higher, in agreement with their larger specific surface area. At higher current densities, the capacitance retention is higher compared to the M5 and M6 sample. This result agrees with higher double layer capacitance and a lower pseudocapacitance, as deduced from the larger S_{av} and lower content of oxygenated functional groups. The samples M13 (open triangles) and M14 (closed triangles) show higher specific capacitances in agreement with their larger S_{av} (843 and 838 m^2 g^{-1}). At low current density, M14 shows higher specific capacitance than M13. This can be explained by: (1) the similar double layer capacitance of both M13 and M14, in agreement with their close S_{av}, and (2) by the higher pseudocapacitive contribution in M14 as a consequence of its higher content in oxygenated functional groups: [CO] = 0.49 mmol g^{-1}

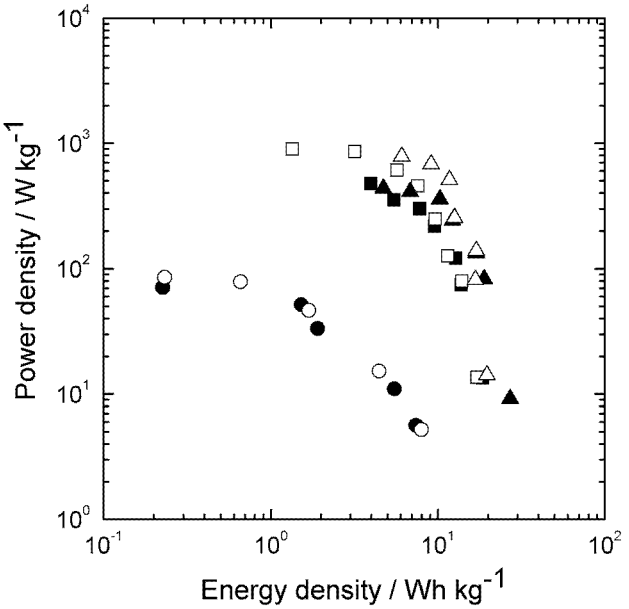

Fig. 6 Power density versus energy density for some activated biocarbons. Symbols stand for as in the caption of Fig. 5

and $[CO_2] = 0.24$ mmol g^{-1} in M13 and $[CO] = 2.77$ mmol g^{-1} and $[CO_2] = 1.95$ mmol g^{-1} in M14. At higher current densities, the capacitance retention is higher in M13, in agreement with its higher double layer capacitance as compared to the pseudocapacitance.

In Fig. 6 the Ragone plot is shown for the samples as those represented in Fig. 5. The energy density (W) was calculated as: $W = \frac{1}{2}\ C \cdot E_2^2$, where C is the specific capacitance and E_2 is the voltage range during the galvanostatic discharge. The power density (P) was calculated as: $P = W/t_d$, where W is the energy density and t_d is the discharge time. The samples M5 and M6 show the lowest energy density and power density, which agree with their low specific capacitances at low current density and their low capacitance retention at high current densities, respectively. The other samples (M1, M2, M13 and M14) display similar P versus W trends, with a maximum energy density (30 Wh kg^{-1}) higher than that for M5 and M6 (11 Wh kg^{-1}). The maximum power density of M1, M2, M13 and M14 (900 W kg^{-1}) is much higher than that of M5 and M6 (80 W kg^{-1}). Both, the higher energy density and higher power density agree with the higher double layer contribution to the overall specific capacitance of the samples M1, M2, M13 and M14 as compared to the samples M5 and M6.

Conclusions

BCs and activated BCs were prepared from *E. grandis* wood dust, an ordinary wood residue. The electrical conductivity of obtained carbons is in the range 10^{-8}–1 S cm^{-1}, showing a sharp variation for the samples that were prepared at temperatures in the range 500–700 °C. The specific capacitance reaches values up to 203 F g^{-1} in acidic electrolyte. The highest specific capacitance was obtained when chemical activation with $ZnCl_2$ at 900 °C followed by chemical oxidation with nitric acid was used. These were the best conditions to achieve high specific surface area and high content of oxygenated functional groups. Good agreement between specific capacitance and both textural properties and surface oxygenated groups content were found. Finally, BCs activated with $ZnCl_2$ at 900 °C and with CO_2 at 800 °C displayed high capacitance retention and high power density. Activation with $ZnCl_2$ at 900 °C also leads to BCs with high energy density.

Acknowledgments Financial support from the projects (MAT 2011-25198 and ANII PR_FSE_2009_1_09) is gratefully acknowledged. A. Cuña thanks the Spanish AECID and Uruguayan ANII for the grants received. V. Barranco thanks the Spanish MINECO for R&C contract. The authors thank Teresa A. Centeno, from INCAR-CSIC, for helpful discussions on the textural characterization of carbons.

References

1. Sharma, P., Bhatti, T.S.: A review on electrochemical double-layer capacitors. Energy Convers. Manag. **51**, 2901–2912 (2010)
2. Chmiola, J., Yushin, G., Gogotsi, Y., Portet, C., Simon, P., Taberna, P.L.: Anomalous increase in carbon capacitance at pore sizes less than 1 nm. Science **313**, 1760–1763 (2006)
3. Conway, B.E.: Electrochemical Supercapacitors. Scientific Fundamentals and Technological Applications. Kluwer Academic, New York (1999)
4. Fuertes, A.B., Pico, F., Rojo, J.M.: Influence of pore structure on electric double-layer capacitance of template mesoporous carbons. J. Power Sources **133**, 329–336 (2004)
5. Pang, H., Wang, S., Li, G., Ma, Y., Li, J., Li, X., Zhang, L., Zhang, J., Zheng, H.: Cu Superstructures fabricated using tree leaves and Cu-MnO_2 superstructures for high performance supercapacitors. J. Mater. Chem. A. **1**, 5053–5060 (2013)
6. Sánchez-González, J., Stoeckli, F., Centeno, T.A.: The role of the electrical conductivity of carbons in the electrochemical capacitor performance. J. Electroanal. Chem. **657**, 176–180 (2011)
7. Inagaki, M., Konno, H., Tanaike, O.: Carbon materials for electrochemical capacitors. J. Power Sources **195**, 7880–7903 (2010)
8. Pandolfo, A.G., Hollenkamp, A.F.: Carbon properties and their role in supercapacitors. J. Power Sources **157**, 11–27 (2006)
9. Barranco, V., Celorrio, V., Lázaro, M.J., Rojo, J.M.: Carbon nanocoils as unusual electrode materials for supercapacitors. J. Electrochem. Soc. **159**(4), A464–A469 (2012)
10. Centeno, T.A., Hahn, M., Fernández, J., Kotz, R., Stoeckli, F.: Correlation between capacitances of porous carbons in acidic and aprotic EDLC electrolytes. Electrochem. Commun. **9**, 1242–1246 (2007)
11. Frackowiak, E., Béguin, F.: Carbon materials for the electrochemical storage of energy in capacitors. Carbon **39**, 937–950 (2001)
12. Ruiz, V., Blanco, C., Raymundo-Piñero, E., Khomenko, V., Béguin, F., Santamaría, R.: Effects of thermal treatment of activated carbon on the electrochemical behaviour in supercapacitors. Electrochim. Acta **52**, 4969–4973 (2007)
13. Centeno, T.A., Stoeckli, F.: The role of textural characteristics and oxygen-containing surface groups in the supercapacitor

performances of activated carbons. Electrochim. Acta **52**, 560–566 (2006)
14. Marsh, H., Rodríguez-Reinoso, F.: Activated Carbons. Elsevier, Oxford (2006)
15. Rufford, T.E., Hulicova-Jurcakova, D., Zhu, Z., Lu, G.Q.: Nanoporous carbon electrode from waste coffe beans for high performance supercapacitors. Electrochem. Commun. **10**, 1594–1597 (2008)
16. Ioannidou, O., Zabaniotou, A.: Agricultural residues as precursors for activated carbon production—a review. Renew. Sustain. Energy Rev. **11**, 1966–2005 (2007)
17. Savova, D., Apak, E., Ekinci, E., Yardim, F., Petrov, N., Budinova, T., Razvigorova, M., Minkova, V.: Biomass conversion to carbon adsorbents and gas. Biomass Bioenergy **21**, 133–142 (2001)
18. Peng, C., Yan, X., Wang, R., Lang, J., Ou, Y., Xue, Q.: Promising activated carbons derived from waste tea-leaves and their application in high performance supercapacitors electrodes. Electrochim. Acta **87**, 401–408 (2013)
19. Rufford, T.E., Hulicova-Jurcakova, D., Zhu, Z., Lu, G.Q.: Microstructure and electrochemical double-layer capacitance of carbon electrodes prepared by zinc chloride activation of sugar cane bagasse. J. Power Sources **195**, 912–918 (2010)
20. Biswal, M., Banerjee, A., Deo, M., Ogale, S.: From dead leaves to high energy density supercapacitors. Energy Environ. Sci. **6**, 1249–1259 (2013)
21. Dubey, S.P., Gopal, K.: Removal of chromium (VI) from contaminated drinking water by ecofriendly adsorbent: equilibrium, isotherm and kinetic study. Water Sci. Technol. **9**(6), 671–679 (2009)
22. Apipreeya, K., Phussadee, P., Prasert, P.: Binary component sorption of Cu (II) and Pb(II) with activated carbon from *Eucalyptus camaldulensis Dehn* bark. J. Ind. Eng. Chem. **15**(4), 465–470 (2009)
23. Phussadee, P., Prasert, P.: Activated carbon from *Eucalyptus camaldulensis Dehn* bark using phosphoric acid activation. Bioresour. Technol. **99**(17), 8540–8543 (2008)
24. Amaya, A., Píriz, J., Tancredi, N., Cordero, T.: Activated carbon pellets from eucaliptus char and tar TG studies. J. Therm. Anal. Calorim. **89**(3), 987–991 (2007)
25. Amaya, A., Medero, N., Tancredi, N., Silva, H., Deiana, C.: Activated carbon briquettes from biomass materials. Bioresour. Technol. **98**(8), 1635–1641 (2007)
26. Centeno, T.A., Sevilla, M., Fuertes, A.B., Stoeckli, F.: On the electrical double-layer capacitance of mesoporous templated carbons. Carbon **43**, 3012–3039 (2005)
27. Setoyama, N., Suzuki, T., Kaneko, K.: Simulation study on the relationship between a high resolution α_s-plot and the pore size distribution for activated carbon. Carbon **36**, 1459–1467 (1998)
28. Kaneko, K., Ishii, C., Ruike, M., Kuwabara, H.: Origin of superhigh area and microcrystalline graphitic structures of activated carbons. Carbon **30**, 1075–1088 (1992)
29. Mora, E., Blanco, C., Pajares, J.A., Santamaría, R., Menéndez, R.: Chemical activation of carbon mesophase pitches. J. Colloid Interf. Sci. **298**, 341–347 (2006)
30. Mochidzuki, K., Soutric, F., Tadokoro, K., Antal Jr, M.J., Toth, M., Zelei, B., Varhegyi, G.: Electrical and physical properties of carbonized charcoals. Ind. Eng. Chem. Res. **42**, 5140–5151 (2003)
31. Shen, W., Li, Z., Liu, Y.: Surface chemical functional groups modification of porous carbon. Recent Pat. Chem. Eng. **1**, 27–40 (2008)
32. Celorrio, V., Calvillo, L., Pérez-Rodríguez, S., Lázaro, M.J., Moliner, R.: Modification of the properties of carbon nanocoils by different treatments in liquid phase. Microporous Mesoporous Mater. **142**, 55–61 (2011)
33. Kennedy, L.J., Vijaya, J.J., Sekaran, G.: Effect of two-stage process on the preparation and characterization of porous carbon composite from rice husk by phosphoric acid activation. Ind. Eng. Chem. Res. **43**, 1832–1838 (2004)
34. Radeke, K.H., Backhaus, K.O., Swiatkowski, A.: Electrical conductivity of activated carbons. Carbon **29**, 122–123 (1991)
35. Hulicova-Jurcakova, D., Puziy, A.M., Poddubnaya, O.I., Suárez-García, F., Tascón, J.M.D., Lu, G.Q.: Highly stable performance of supercapacitors from phosphorous-enriched carbons. J. Am. Chem. Soc. **131**, 5026–5027 (2009)
36. Nian, Y., Teng, H.: Nitric acid modification of activated carbon electrodes for improvement of electrochemical capacitance. J. Electrochem. Soc. **149**(8), A1008–A1014 (2002)